CDF Note 11167

Measurement of $W \to \ell\nu$ + jets Production Cross Sections

The CDF Collaboration
URL http://www-cdf.fnal.gov
(Dated: July 14, 2015)

Preliminary results for the production of a W-boson in association with jets, in $p\bar{p}$ collisions at $\sqrt{s}$=1.96 TeV center mass energy are presented. The measurements are based on the entire Run II data set collected by CDF, which corresponds to an integrated luminosity of 9.0 fb^{-1}. Cross sections for the inclusive production of jets with $E_T^{jet} > 25$ GeV and $|\eta^{jet}| < 2$, in conjunction with a W boson which decays into an electron-neutrino or muon-neutrino pair, are presented as a function of E_T^{jet} and jet multiplicity.

I. INTRODUCTION

The measurement of the production of jets in association with a W-boson in $p\bar{p}$ collisions allows for precision tests of perturbative Quantum ChromoDynamics (QCD). Moreover, the W+jets final state is also one of the main backgrounds for important standard model (SM) processes like, for example, $t\bar{t}$, single-top and Higgs boson production and for a variety of physics processes beyond the SM. Therefore, it is crucial to accurately measure this process. We report on preliminary measurement of $W(\rightarrow \ell\nu)$+jets production (where $\ell = e, \mu$) using 9.0 fb^{-1} of data collected with the CDF detector in Run II. The CDF detector is described in detail in [1]. This measurement follows previous studies of jet pairs produced in association with a W-boson at CDF [2]. The measured cross sections are unfolded back to particle level and compared to theoretical perturbative QCD (pQCD) predictions. Measurements of inclusive jet differential cross section as a function of the leading jet E_T [3], in events with at least one jet in the final state, and of the total cross sections as a function of inclusive jet multiplicity are presented.

II. DATA SAMPLE & EVENT SELECTION

This analysis is based on the entire Run II dataset collected with the CDF detector. The data are collected by using an inclusive lepton trigger that selects events with at least one electron with E_T >18 GeV or a muon with p_T >18 GeV/c. Offline, from this inclusive lepton dataset, the events with a W boson that decays leptonically (only $W \rightarrow e\nu$ and $W \rightarrow \mu\nu$ are considered as signal) are identified by requiring the presence of exactly one reconstructed isolated central (*i.e.* $|\eta^\ell| < 1.0$) electron candidate with E_T greater than 25 GeV or muon with p_T greater than 25 GeV/c. To reduce the QCD background from multijets production we require that the transverse mass of the W boson candidate is greater than 40 GeV:

$$m_T^W = \sqrt{2p_T^\ell \not\!\!E_T[1 - \cos(\Delta\phi(\ell, \not\!\!E_T))]} > 40 \text{ GeV}, \quad (1)$$

where $\not\!\!E_T$ is the missing transverse energy [4] and $\Delta\phi(\ell, \not\!\!E_T)$ is the azimuthal separation between the momentum vector of the lepton ($\ell = e$, the electron or μ, the muon) and the $\not\!\!E_T$.

In addition to the W-boson candidate, al least one jet with $E_T > 25$ GeV, pseudorapidity $|\eta| < 2$ and electromagnetic fraction lower than 0.9 is required. Jets are reconstructed using the JETCLU cone algorithm [5] with jet radius parameter $R = \sqrt{\Delta\phi^2 + \Delta\eta^2} = 0.4$. The energy of each jet is corrected by using the jet energy scale (JES) correction described in detail in [6]. In addition, we account for the differences in the response to particle showers which originate from gluons and those which originate from quarks (quark/gluon jets) in simulated events [2]. In order to consider only well-separated jets, jets close to the W decay lepton ($\Delta R(\ell, jets) < 0.4$) are not considered.

III. BACKGROUND MODELING & VALIDATION

The sample of events selected from data is expected to include a number of background events. These backgrounds can be divided into two categories that we refer to as "physics processes" and "multijet production".

The physics processes are backgrounds with real leptons (electrons or muons) from boson decay in the final states. Included in these categories are the final states $W(\rightarrow \tau\nu)$+jets, $Z \rightarrow \ell^+\ell^-$+jets, top quark production ($t\bar{t}$ and single top), WW, WZ and ZZ. All these processes are simulated using Monte Carlo techniques. Among these backgrounds, $Z(\rightarrow \ell^+\ell^-)$+jets is the dominant background at low ($n = 1,\ 2$) jet multiplicity, while top quark pair production is the primary background at high ($n = 3,\ 4$) jet multiplicity. Z+jets and $W(\rightarrow \tau\nu)$+jets events are generated using ALPGEN [8] interfaced with PYTHIA [7] parton showering and hadronization algorithms. Top-quark pair production is modeled, assuming a top-quark mass of 172.5 GeV/c^2, with the PYTHIA event generator. Single-top processes (both s-channel and t-channel) are modeled with events simulated by the MADEVENT [9] generator followed by the use of PYTHIA parton showering and hadronization models. WW, WZ and ZZ production are modeled with PYTHIA Monte Carlo calculation. The expected contributions of each process are normalized based on the theoretical cross section. The rate of associated production of W and Z (WW, WZ, ZZ) is scaled to the cross-section calculated to next-to-leading order (NLO) [10], the $t\bar{t}$ sample is normalized using an approximate next-to-next-to-leading order plus next-to-next-to-leading logarithm (NNLO+NNLL) [11] cross-section calculation, the single-top process is normalized to approximate next-to-next-leading order plus next-to-next-to-leading logarithm (NNLO+NNLL) calculations [12] for the s-channel and approximate next-to-next-to-leading order plus next-to-leading logarithm (NNLO+NLL) calculations [13] for the t-channel, and the Z+jets and W+jets are normalized to leading order (LO) calculations and scaled by an additional K-factor of 1.4 to account for next-to-leading order effects [14]

and [15]. The resulting uncertainties on each background contribution are 6% for the WW, WZ and ZZ, 3% and 11% for top quark pair production and single top quark production, respectively, 20% and 40% for $Z \to \ell^+\ell^- +$jets and $W(\to \tau\nu)$+jets. The background normalization is also affected by systematic uncertainties in the integrated luminosity measurement (6%), the lepton acceptance (2.2%) and the JES (2.7% for quark jets and 4.4% gluon jets with the two components being 100% anti correlated [2]). The multijet background events enter the signal sample when one of the jets is misidentified as a lepton. This background is the largest background contribution in the electron channel, but negligible for the muon channel since it is less likely for a jet to result in a fake muon candidate. In both channels it is modeled using a data-driven method. The data samples used to model the multijet background are obtained from the same dataset described in section II by requiring that two (one) of the electron (muon) identification criteria fail.

The electron candidates with the two inverted identification criteria are referred to as "nonelectrons" [2]. The requirements to be inverted are chosen in such a way that the nonelectron sample is kinematically similar to the signal sample but statistically independent. Moreover, in order to adequately model the multijet component, we apply the same tuning procedure as that described in [2]. First, the contamination from the processes with a real lepton are removed statistically from the nonelectron sample by subtracting them bin-by-bin in the variable of interest using the theoretical predictions for that bin. Second, in order to correctly model the kinematic proprieties of the event, the E_T of the nonelectron is determined by the E_T of the corresponding jet (*i.e.* the jet with $\Delta R < 0.4$ with respect to the nonelectron). The E_T of the jet matched to nonelectron is also corrected for the difference in jet-energy scale between the jet producing the nonelectron and the jet producing a misidentified electron, *i.e.*, the jet fulfilling all the electron selection criteria ("nonelectron energy scale correction") and the discrepancies due to a bias arising from the trigger ("trigger bias correction").

To correct the nonelectron transverse energy we use the same energy scale correction as was previously evaluated for the $W + 2$ jets sample [2]. The results of repeating the same studies on the $W+ \geq 1$ jet sample are in agreement within the uncertainties quoted. We therefore used them to define the systematic uncertainties in the corrections. Another effect considered as a systematic uncertainty of this correction is that it is an average correction and does not account for the energy resolution.

The trigger bias correction is evaluated in a control region defined by reversing the W-boson transverse mass requirement. To account for the possible dependence of the correction on the choice of the control region we derived two sets of corrections from two non-overlapping control regions: $m_T^W < 20$ GeV and 20 GeV $\leq m_T^W \leq 40$ GeV. The two sets of corrections are then applied to the whole control region and the differences with respect to the nominal distribution are assigned as an uncertainty to the nominal correction.

The muon channel multijet background is modeled using muon candidates that pass all the muon requirements but with isolation [16] between 0.1 and 0.2, rather than the customary 0.1. We refer to these muons as "almost-isolated muons". Events with isolation greater than 0.2 are used to evaluate a systematic uncertainty on the model.

The multijet background rate expected in the signal region ($N_{MJ}|_{SR}$) is estimated using equation 2:

$$N_{MJ}|_{SR} = \frac{N_{MJ}|_{CR}}{N_{MJ}|_{MJCR}} \cdot N_{MJ}|_{MJSR}, \tag{2}$$

where $N_{MJ}|_{MJCR}$ and $N_{MJ}|_{MJSR}$ are the number of events in CR and in SR, respectively, that have passed the nonelectron or almost-isolated muon selections after the removal of the contribution from the processes with real leptons, as previously explained, and $N_{MJ}|_{CR}$ is the number of multijet events expected in the control region chosen by reversing the W boson transverse mass requirement. The expected multijet events in the analysis control region ($N_{MJ}|_{CR}$) is the number of data events in the control region sample ($N_{DATA}|_{CR}$) minus the number of expected Monte Carlo simulated background ($N_{MC}|_{CR}$) and signal ($N_{WJETS}|_{CR}$) contributions:

$$N_{MJ}|_{CR}=(N_{DATA} - N_{MC} - N_{WJETS})|_{CR}. \tag{3}$$

To avoid circularity, $N_{WJETS}|_{CR}$ is estimated using the measured cross-section σ^{meas}_{WJETS}, instead of the theoretical calculation. The process is iterative: since, to first order, the control region is composed entirely of multijet events, we start with the approximation:

$$N_{MJ}|_{CR}=N_{DATA}|_{CR} \tag{4}$$

and we calculate σ^{meas}_{WJETS} using equation:

$$\sigma^{meas}_{WJETS} = \frac{N_{DATA}|_{SR} - N_{MC}|_{SR} - N_{MJ}|_{SR}}{L\,\mathcal{A}_{SR}\,\epsilon} \tag{5}$$

where $L\,\mathcal{A}_{SR}\,\epsilon$ is the product of the integrated luminosity, the acceptance in the signal region and the trigger efficiency; $N_{MC}|_{SR}$ is the estimated number of Monte Carlo simulated background in the signal region and $N_{MJ}|_{SR}$ is evaluated

by replacing $N_{MJ}|_{CR}$ of equation 4 into equation 2. $N_{WJETS}|_{CR}$ is then calculated by using σ^{meas}_{WJETS}. The next order approximation of $N_{MJ}|_{CR}$ is then calculated with the measured $N_{WJETS}|_{CR}$. The process is iterated until the multijet scale factor f^{ℓ}_{MJ} defined by equation:

$$f^{\ell}_{MJ} = \frac{N_{MJ}|_{CR}}{N_{MJ}|_{MJCR}} \tag{6}$$

does not change by more than 1%.

The same control region is used to validate the model. Figure 1 shows that data and model are in agreement within uncertainty in this region.

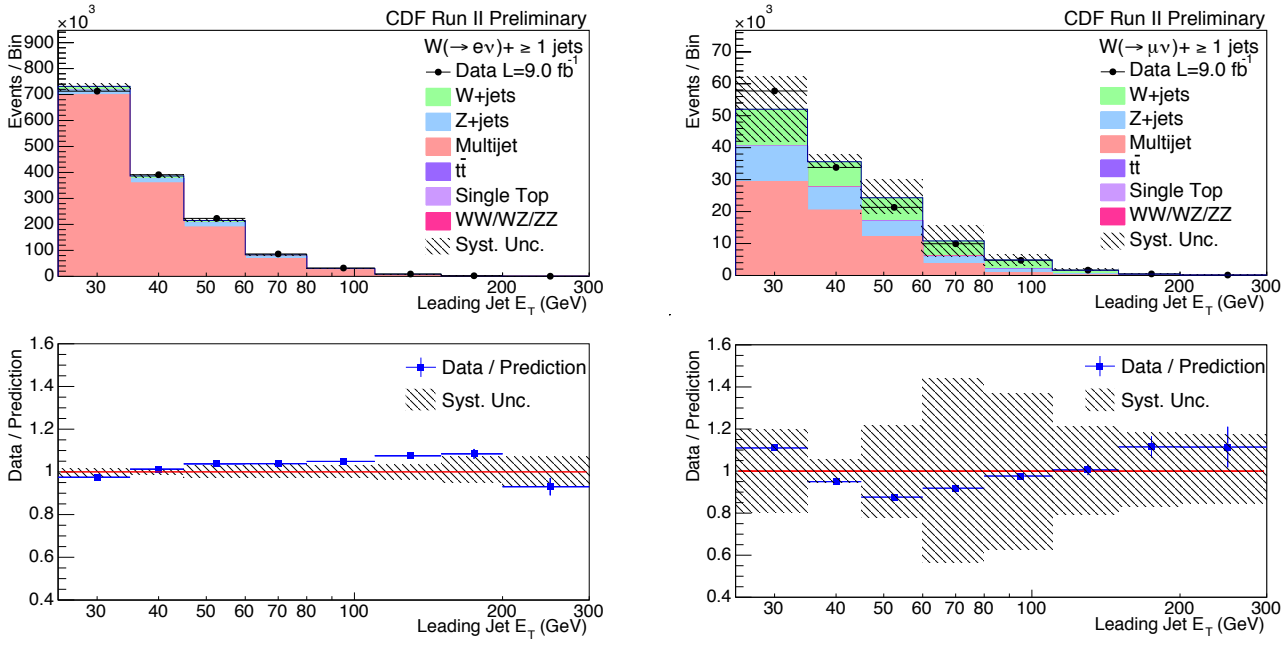

(a) (b)

FIG. 1: The leading jet E_T distribution for the $W(\to e\nu)+ \geq 1$ jets sample (a) and $W(\to \mu\nu)+ \geq 1$ jets sample (b) in the control region. The lower figures illustrate the ratio between data and prediction.

IV. CROSS SECTION MEASUREMENT

The measured differential cross section per bin of a variable α, which in this note is either the number of jets or the E_T of the leading jet, is defined as:

$$\frac{\Delta\sigma^{meas}_{W\to\ell\nu+jets}}{\Delta\alpha} = \frac{1}{\Delta\alpha}\, U(\alpha)\, \frac{N_{DATA}(\alpha) - N_{BKG}(\alpha)}{L} \tag{7}$$

where $\Delta\alpha$ is the width of the bin in which the cross section is measured, $N_{DATA}(\alpha) - N_{BKG}(\alpha)$ represents background subtraction, $U(\alpha)$ is the unfolding factor and L is the integrated luminosity. In each bin the number of estimated background events $N_{BKG}(\alpha)$, is subtracted from the $W+$jets yield in data, $N_{DATA}(\alpha)$. Then the unfolding factor $U(\alpha)$ is applied to remove all the detector effects and to unfold the measurement back to the particle level for direct comparison with the theoretical predictions. Details on the background subtraction and on the unfolding procedure are reported in Sections IV A and IV B, respectively.

A. Background Subtraction

The yield of estimated background and data events for $W+ \geq 1,\ 2,\ 3$ and 4 jets are reported in Tables I and II, for the electron and the muon channel, respectively.

CDF Run II Preliminary
Estimated and Observed Number of Events in 9.0 fb^{-1} $W(\rightarrow e\nu)+$jets

Backgrounds	≥ 1 jet	≥ 2 jets	≥ 3 jets	≥ 4 jets
Multijet	142382 ± 23500	21706 ± 2783	3022 ± 427	470 ± 68
Z+jets	21959 ± 4392	2771 ± 554	348 ± 70	41 ± 8
$W(\rightarrow \tau\nu)$+jets	8717 ± 3487	948 ± 379	99 ± 40	10 ± 4
WW, WZ, ZZ	3759 ± 229	1693 ± 103	231 ± 14	31 ± 2
$t\bar{t}$	2769 ± 83	2535 ± 76	1756 ± 53	736 ± 22
Single Top	2038 ± 228	1187 ± 133	243 ± 27	33 ± 4
Total Backgrounds	181624 ± 24162	30840 ± 2869	5699 ± 438	1321 ± 72
Data	477665	65029	9483	1642

TABLE I: Estimated background events in 9.0 fb^{-1} for $W(\rightarrow e\nu)+ \geqslant 1$, 2, 3 and 4 jets and data yields.

CDF Run II Preliminary
Estimated and Observed Number of Events in 9.0 fb^{-1} $W(\rightarrow \mu\nu)+$jets

Backgrounds	≥ 1 jet	≥ 2 jets	≥ 3 jets	≥ 4 jets
Z+jets	23287 ± 4657	2600± 520	275 ± 55	29 ± 6
$W(\rightarrow \tau\nu)$+jets	4571± 1828	496 ± 199	48 ± 19	5 ± 2
Multijet	6407 ± 990	716 ± 291	129 ± 80	13 ± 13
WW, WZ, ZZ	2430 ± 146	1102 ± 66	146 ± 9	18 ± 1
$t\bar{t}$	1739 ± 52	1593 ± 48	1101 ± 33	462 ± 14
Single Top	1317 ± 149	767 ± 85	156 ±18	22 ± 3
Total Backgrounds	39751 ± 5104	7274 ± 639	1855 ± 106	549 ± 20
Data	229823	28038	3967	807

TABLE II: Estimated background events in 9.0 fb^{-1} for $W(\rightarrow \mu\nu)+ \geqslant 1$, 2, 3 and 4 jets and data yields.

The total background fraction increases with the jet multiplicity. As anticipated the multi-jet process is the main background for the electron channel while the Z+jets and $t\bar{t}$ backgrounds dominate in the muon channel. In both channels, the estimated fraction of multijet events decreases with increasing jet multiplicity. The $t\bar{t}$ background contribution is the largest single contribution for the samples with $\geqslant 3$ and $\geqslant 4$ jets. The contribution of the WW, WZ, ZZ and the single-top backgrounds grow in the $\geqslant 2, 3, 4$ jet multiplicities but is almost negligible in both channels. These observations are presented in figure 2 in which the comparison between the inclusive number of jets in reconstructed data and in signal (theoretical prediction generated with ALPGEN+PYTHIA Monte Carlo calculation and normalized to LO×K-factor) plus background for $W(\rightarrow e\nu)+ \geqslant N$ jets and $W(\rightarrow \mu\nu)+ \geqslant N$ jets, jets are shown.

B. Unfolding Procedure

In order to facilitate comparison with theoretical predictions, the particle level cross section is determined from the measured rates using an unfolding procedure. The cross section at particle level can be evaluated by correcting the measurement for all the detector effects, such as finite resolution and limited acceptance, that can distort the distribution under study. This unfolding procedure takes into account migration of events from one jet multiplicity to another due to resolution and acceptance effects. The unfolding can be accomplished by evaluating the response matrix ($\mathcal{M}_{ij}$) that maps the particle level distribution T_j to the reconstructed distribution R_i:

$$R_i = \sum_j \mathcal{M}_{ij}\ T_j. \tag{8}$$

Ideally, the unfolded distribution can then be obtained by applying the inverted matrix $\mathcal{M}^{-1}$ to the measured data (background subtracted data). Inversion of the the non-diagonal response matrix $\mathcal{M}$ requires special care since low-significance (low statistics) bins can introduce numerical instabilities. To avoid such problems, the measured

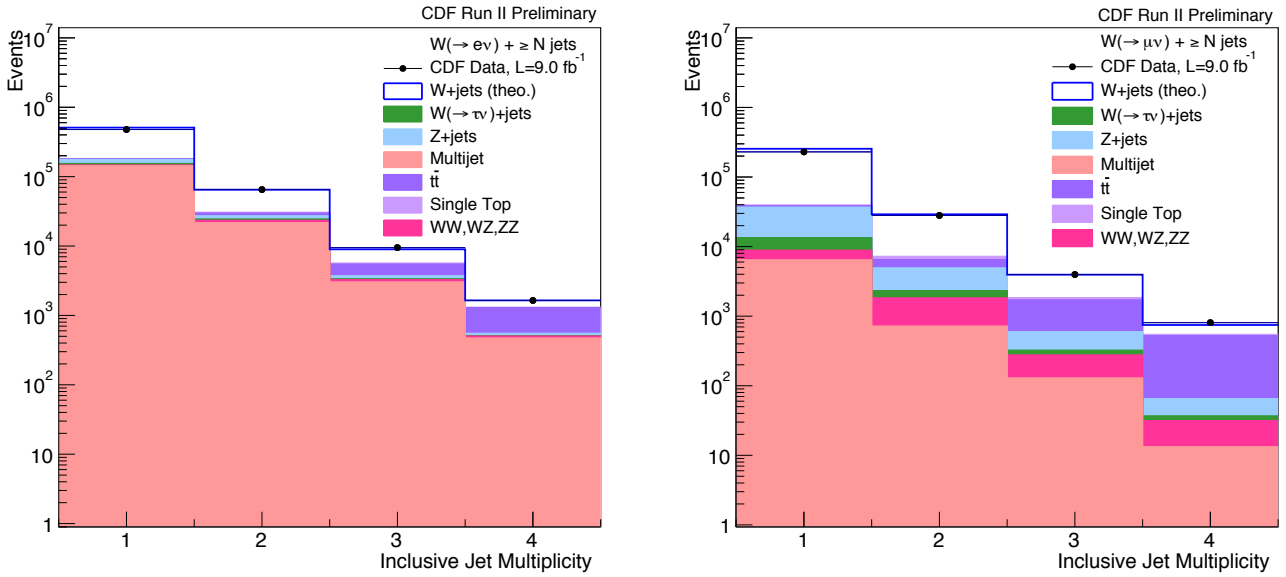

(a) (b)

FIG. 2: Data and background jet multiplicities in the $W \to e\nu$ channel (a) and in the $W \to \mu\nu$ channel (b). The LO×K-factor ALPGEN+PYTHIA theoretical prediction is also shown.

distributions are unfolded with the regularized singular value decomposition (SVD) technique [18]. In this analysis the migration matrix for each measurement is derived using the $W+$jets sample generated with ALPGEN+PYTHIA. Each entry (i, j) of the matrix corresponds to the number of reconstructed events in bin i that are generated in bin j at particle level. The particle level jets are reconstructed in the Monte Carlo simulated sample by applying the JETCLU algorithm to the stable particles of the HEPG bank in the final states. The same analysis requirements applied to jets and the lepton at detector level are applied at particle level. Events falling outside the analysis phase space are rejected. The resulting inefficiency is quantified bin-by-bin in a diagonal acceptance matrix.

V. SYSTEMATIC UNCERTAINTIES

In this analysis, we considered the uncertainties in the background estimation and those in the unfolding procedure as systematic uncertainties. The unfolding procedure is repeated for each systematic variation, and the difference between unfolded data and nominal result is taken as uncertainty. Figures 3 and 4 show the systematic uncertainties as a function of inclusive jet multiplicity and first jet transverse energy in both electron and muon channels. The uncertainties in the background estimation include the uncertainties in the Monte Carlo simulated background normalization (MC backgrounds), the uncertainty in the lepton acceptance (Acceptance), the uncertainty in the jet energy scale (JES) and the uncertainties in the estimation of the number of multijet background events (MJ background). These sources of systematic uncertainties are discussed in detailed in section III. The systematic uncertainty in the unfolding procedure is assessed by performing one thousand simulated experiments. The uncertainty assigned to the unfolding procedure is the width of the distribution of the residual calculated for each bin in which the differential cross-section is measured. We also account for the lepton acceptance (2.2%) and resolution (JES) uncertainties in the $W+$jets simulated events used to build the unfolding matrix by properly accounting for all the correlations.

VI. CHANNEL COMBINATION

$W+$jets cross sections are measured independently in the electron and muon decay channels. These are combined using the Best Linear Unbiased Estimates method [19]. The algorithm used, the Asymmetric Iterative BLUE (AIB) [20], takes into account possible correlations of the uncertainties in the two channels. Systematic uncertainties related to JES, MC background and luminosity are considered 100% correlated. On the other hand, statistical, trigger

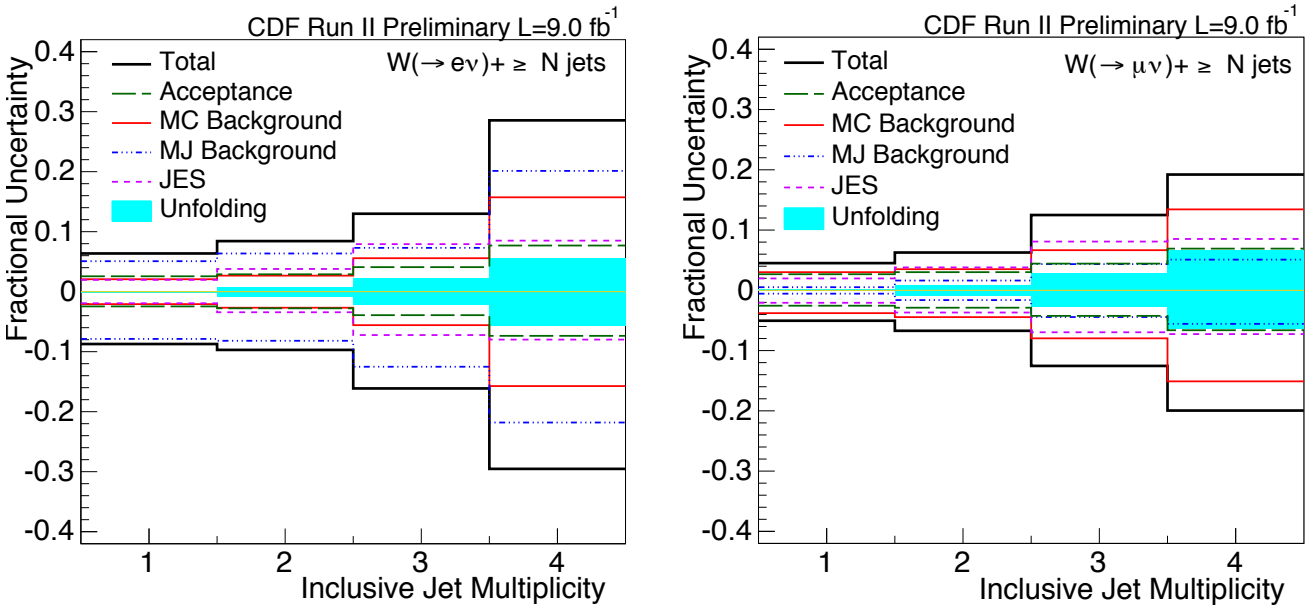

(a) (b)

FIG. 3: Total systematic uncertainties vs inclusive jet multiplicity in the $W \to e\nu$ channel (a) and in the $W \to \mu\nu$ channel (b).

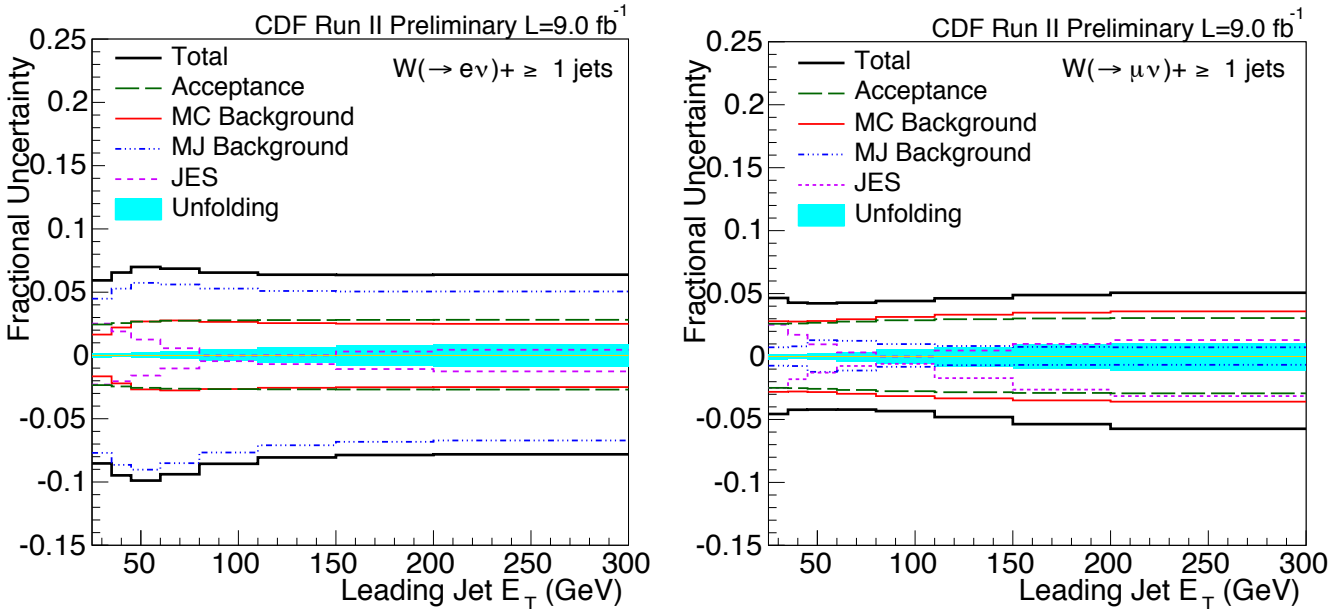

(a) (b)

FIG. 4: Total systematic uncertainties vs leading jet E_T in the $W \to e\nu$ channel (a) and in the $W \to \mu\nu$ channel (b).

efficiency and multijet background uncertainties are considered uncorrelated. The algorithm accounts also for possible asymmetric errors. Results are shown in figure 5.

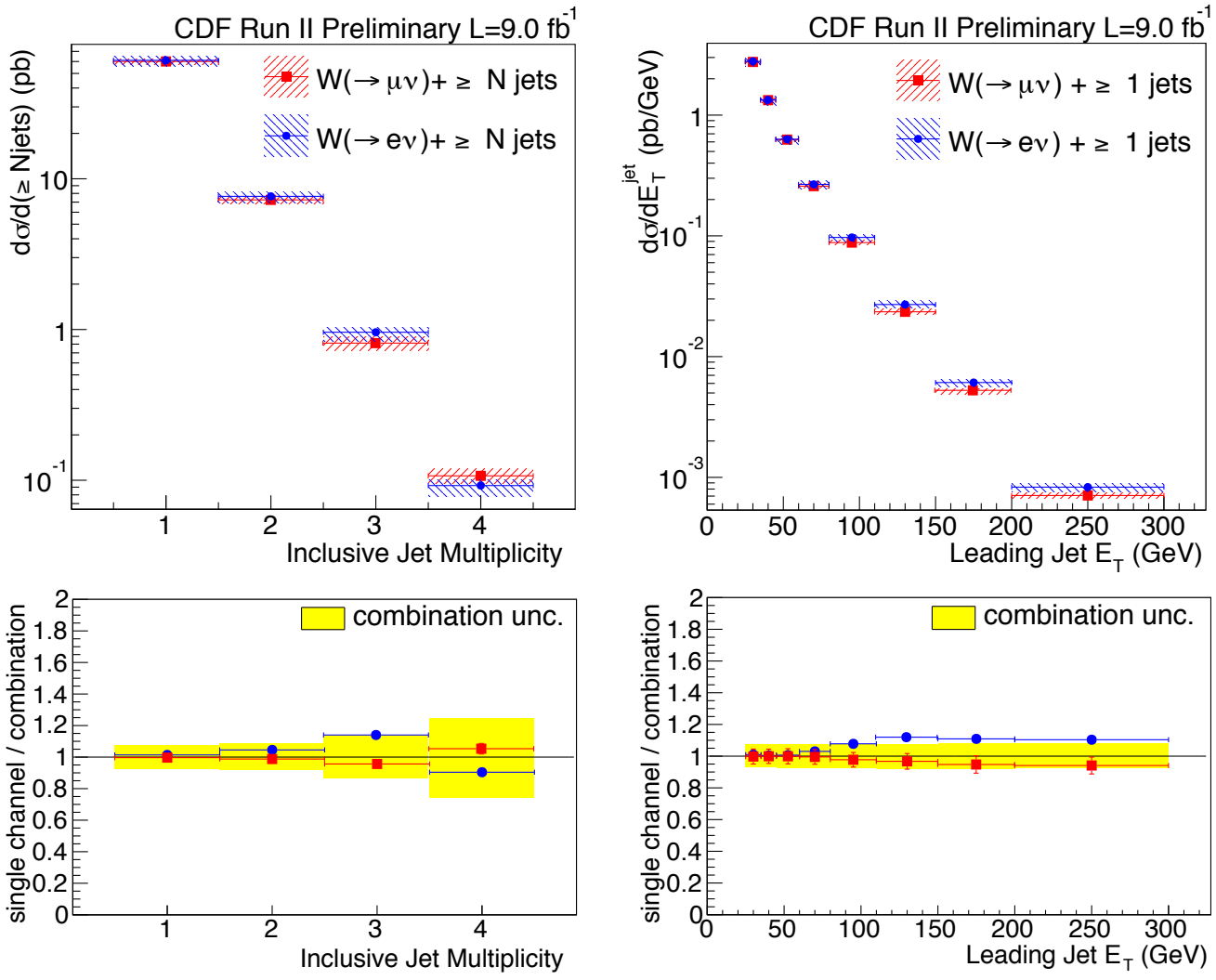

(a) (b)

FIG. 5: Measured cross section in the $W(\rightarrow e\nu)$+jets (blue dots) and $W(\rightarrow \mu\nu)$+jets (red squares) decay channels as a function of inclusive number of jets (a) and inclusive leading jet E_T (b) in events with ≥ 1 jet. The lower figures illustrate the ratio between measured cross sections and combination with the total systematic uncertainty (all correlations are properly accounted for).

VII. THEORETICAL PREDICTIONS

The cross sections measured at particle level are compared with ALPGEN+PYTHIA predictions. ALPGEN is used to simulate the associated production of the W-bosons plus n partons and PYTHIA performs the showering and hadronization. The cross section is a leading order prediction scaled up by a K-factor of 1.4 to account for the next to leading order effects [15]. The Parton Distribution Function, PDF, used is the leading order CTEQ5L set and the nominal choice of the renormalization and factorization scale is $\mu_0 = \sqrt{m_W^2 + P_T^2}$ where P_T^2 is the squared sum of transverse energies of all final state partons. The PDF uncertainties are obtained using the Hessian method [21]. The uncertainty due to the choice of the renormalization and factorization scale is defined by the predictions with $\mu_0/2$ and $2\mu_0$ as shown with the data in figure 6. This uncertainty in the theoretical cross section is large since the leading order predictions suffer from dependence on the choice of the renormalization scale.

VIII. RESULTS

The cross sections as a function of jet multiplicity and the first leading jet E_T are shown in figure 6. The measurements refer to particle level cross sections with one central ($|y|$ <1) lepton and at least one jet with $E_T > 25\,\text{GeV}$ and rapidity $|y|$ <2. In addition the reconstructed transverse mass of the W-boson must be more then 40 GeV. For comparison, the LO×K-factor ALPGEN+PYTHIA predictions are included in each figure.

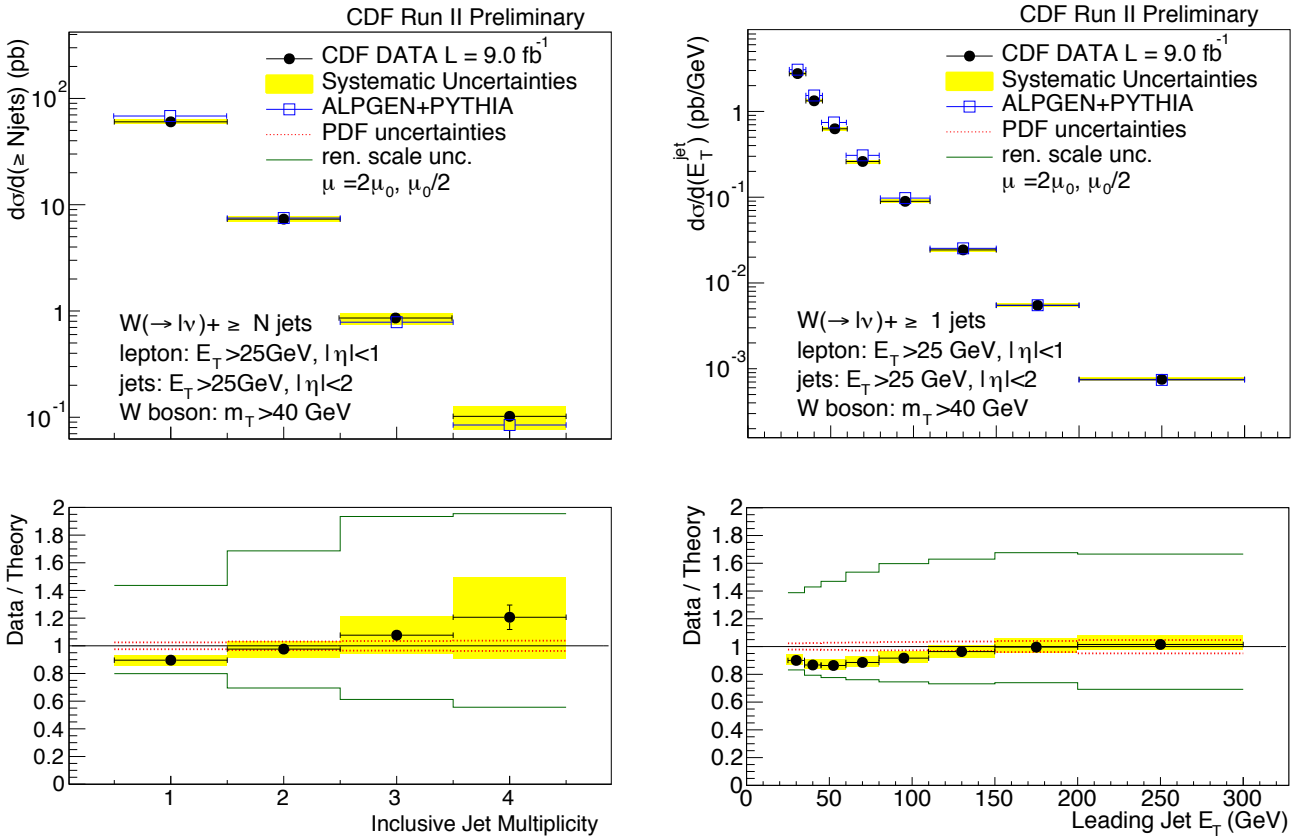

(a) (b)

FIG. 6: Measured inclusive jet differential cross section (black dots) as a function of the inclusive jet multiplicity (a) and leading jet E_T (b) compared to LO calculations corrected by K-factor pQCD predictions (open squares). The shaded bands show the total systematic uncertainty, except for the 6% luminosity uncertainty. The dashed and the solid lines indicate the PDF uncertainty and the variation of the renormalization scale μ_0, respectively.

Figure 6a shows the measured cross section as a function of inclusive $W(\to \ell\nu)+ \geq N$ jets multiplicity up to $N = 4$. The systematic uncertainties on the measured cross sections are mainly due to the background modeling and are of the order of 8% for $N \geq 1$ jet up to 28% for $N \geq 4$ jets. Table III provides the corresponding numerical results for each measured inclusive jet cross section.

Figure 6b presents the measured differential cross section as a function of the leading jet E_T in $W(\to \ell\nu)+ \geq 1$ jets events. The differential cross section is measured in eight bins of leading jet E_T in the range 25 GeV to 300 GeV. The cross sections decrease by approximately three orders of magnitude as the leading jet E_T increases from 30 to 300 GeV. The systematic uncertainty on the measured cross sections is about 5% and is mainly due to the background modeling.

It is clear from the bottom plots of Fig. 6 that, when comparing the measured cross sections with the theoretical predictions, the main theoretical uncertainty comes from the scale (renormalization and factorization) variation. This scale uncertainty reflects the uncertainty connected with missing higher order corrections. Given the superior accuracy of these measurements, comparison with higher order calculations is very desirable.

CDF Run II Preliminary, L=9.0 fb^{-1}

$W(\to \ell\nu)+ \geq N$ jet [$E_T^\ell > 25\,\text{GeV}$, $|\eta^\ell| < 1$, $E_T^{jet} > 25\,\text{GeV}$, $|\eta^{jet}| < 2$ and $m_T^W > 40\,\text{GeV}$]

Jet Multiplicity	**Inclusive σ [pb]**
≥ 1 jet	$60.3 \pm 0.1\,(\text{stat.})^{+2.7}_{-2.6}(\text{syst.}) \pm 3.6\,(\text{lum.})$
≥ 2 jets	$7.31 \pm 0.04\,(\text{stat.})^{+0.43}_{-0.44}(\text{syst.}) \pm 0.44\,(\text{lum.})$
≥ 3 jets	$0.84 \pm 0.02\,(\text{stat.})^{+0.10}_{-0.11}(\text{syst.}) \pm 0.05\,(\text{lum.})$
≥ 4 jets	$0.102 \pm 0.007\,(\text{stat.})^{+0.024}_{-0.026}(\text{syst.}) \pm 0.006\,(\text{lum.})$

TABLE III: The unfolded $W(\to \ell\nu)$ + jets cross section measurements for inclusive jet multiplicities up to 4 jets together with statistical, systematic and luminosity uncertainties. The kinematic region to which the measurements are restricted is $E_T^\ell > 25\,\text{GeV}$, $|\eta^\ell| < 1$, $E_T^{jet} > 25\,\text{GeV}$, $|\eta^{jet}| < 2$ and $m_T^W > 40\,\text{GeV/c}^2$.

IX. CONCLUSIONS

Cross section measurements for the production of jets in association with a W-boson, based on the full dataset collected with the CDF experiment at the Tevatron which corresponds to an integrated luminosity of 9.0 fb^{-1}, are presented. The W-bosons are identified through their leptonic decays to electrons and muons. The cross sections of the $W(\to e\nu)$ and $W(\to \mu\nu)$ are unfolded to particle level and then combined. Measurements are performed in the kinematic region $E_T^\ell > 25\,\text{GeV}$, $|\eta^\ell| < 1$, $E_T^{jet} > 25\,\text{GeV}$, $|\eta^{jet}| < 2$ and $m_T^W > 40\,\text{GeV/c}^2$ and jets are reconstructed with JETCLU algorithm. The measured cross-section as a function of the inclusive jet multiplicity and the leading jet E_T are presented. Experimental uncertainties are of the order of 8% for $N \geq 1$ jet up to 28% for $N \geq 4$ jets, and about 5% for all the leading jet E_T range considered. The main experimental uncertainty is associated with the background modeling. Cross sections are compared with theoretical predictions from ALPGEN interfaced with PYTHIA. The dominant uncertainty in the theoretical prediction is related to the variation of the renormalization and factorization scale. The LO×K-factor ALPGEN+PYTHIA predictions are consistent with the measured cross sections, but this comparison is limited by the large systematic uncertainties associated with the theoretical predictions.

Acknowledgments

We thank the Fermilab staff and the technical staffs of the participating institutions for their vital contributions. This work was supported by the U.S. Department of Energy and National Science Foundation; the Italian Istituto Nazionale di Fisica Nucleare; the Ministry of Education, Culture, Sports, Science and Technology of Japan; the Natural Sciences and Engineering Research Council of Canada; the National Science Council of the Republic of China; the Swiss National Science Foundation; the A.P. Sloan Foundation; the Bundesministerium für Bildung und Forschung, Germany; the Korean World Class University Program, the National Research Foundation of Korea; the Science and Technology Facilities Council and the Royal Society, UK; the Russian Foundation for Basic Research; the Ministerio de Ciencia e Innovación, and Programa Consolider-Ingenio 2010, Spain; the Slovak R&D Agency; the Academy of Finland; the Australian Research Council (ARC); and the EU community Marie Curie Fellowship contract 302103.

[1] F. Abe *et al.*, Nucl. Instrum. Methods Phys. Res. A **271**, 387 (1988); D. Amidei *et al.*, Nucl. Instum. Methods Phys. Res. A **350**, 73 (1994); F. Abe *et al.*, Phys. Rev. D **52**, 4784 (1995); P. Azzi *et al.*, Nucl. Instrum. Methods Phys. Res. A **360**, 137 (1995); The CDFII Detector Technical Design Report, Fermilab-Pub-96/390-E; D. Acosta *et al.* (CDF Collaboration), Phys. Rev. D **71**, 032001 (2005).

[2] T. Altonen et al. (CDF Collaboration), Phys. ReV. D **89**, 092001 (2014).

[3] Coordinates are referred to a cylindrical system with the z axis along the beam line, polar angle θ and azimuthal angle ϕ. Transverse energy and momentum are defined as $E_T = E\sin\theta$ and $p_T = p\sin\theta$, pseudo-rapidity as $\eta = -\ln(\tan\frac{\theta}{2})$ and rapidity as $y = \frac{1}{2}\ln(\frac{E+p_z}{E-p_z})$.

[4] The missing transverse energy is calculated as the transverse vector sum of all calorimeter-tower energy depositions and includes the corrections for the jet energies and for the momenta of the muons.

[5] F. Abe et al. (CDF Collaboration), Phys. ReV. D **45**, 1448 (1992).
[6] A. Bhatti *et al.*, Nucl. Instrum. Methods Phys. Res. A **566**, 375 (2006).
[7] T. Sjostrand *et al.*, Comput. Phys. Commun. **135**, 238 (2001).
[8] M. L. Mangano *et al.*, J. High Energy Phys. **07**, 001 (2003).
[9] F. Maltoni and T. Stelzer, J. High Energy Phys. **02**, 27 (2003).
[10] J. M. Campbell and R. K. Ellis, Phys. Rev. D **60**, 113006 (1999).
[11] M. Czakon, P. Fiedler, A. Mitov , Phys. Rev. Lett. **110** (2013) 252004.
[12] N. Kidonakis, Phys. Rev. D **81**, 054028 (2010).
[13] N. Kidonakis, Phys. Rev. D **83**, 091503 (2011).
[14] Aaltonen T. *et al.* (CDF Collaboration), Phys. Rev. D **79**, 052008 (2009).
[15] Aaltonen T. *et al.* (CDF Collaboration), Phys. Rev. D **82**, 112005 (2010).
[16] Isolation is defined as the calorimeter transverse energy in a cone of opening $\Delta R \equiv \sqrt{(\Delta\eta)^2 + (\Delta\phi)^2} = 0.4$ around the lepton (not including that of the lepton energy itself) divided by the lepton E_T (for the electron) or p_T (for the muon).
[17] H. L. Lai *et al.*, Eur. Phys. J. C **12**, 375 (2000).
[18] A. Höcker, V. Kartvelishvili, Nucl. Instrum. Meth. A **372**, 469 (1996).
[19] L. Lyons and D. Gibaut and P. Clifford, Nucl. Instr. and Meth. A **270**, 110 (1988).
[20] R. Group, C. Ciobanu, K. Lannon, and C. Plager (CDF Collaboration), in Proceedings of the 34th International Conference in High Energy Physics (ICHEP08), Philadelphia, 2008, eConf C080730, arXiv:0809.4670 [hep-ex].
[21] J. Pumplin *et al.*, J. High Energy Phys. **0207**, 012 (2002).